LANGMUIR

pubs.acs.org/Langmuir Article

Motion of Droplets in Lyophilic Axially Varying Geometry-Gradient Tubes

Zhiqiang Xiao, Xiaoling Hu, Di Wu,* and Kui Song*

Cite This: *Langmuir* 2023, 39, 7901−7911 Read Online

ACCESS | Metrics & More | Article Recommendations | Supporting Information

ABSTRACT: Droplet transport occurs frequently in nature and has a wide range of applications. We studied the droplet motion in a lyophilic axially varying geometry-gradient tube (AVGGT). The motion of the AVGGT in two directions—from the large opening side (L) to the small opening side (S) and from S to L—was theoretically and experimentally analyzed. The droplet dynamic behaviors, such as the self-transport behavior and the droplet stuck behavior, are explored from the view points of mechanics and energy. We found that the surface tension force of a three-phase contact line can be either a driving or an impeding force depending on the various droplet geometries in different AVGGTs. An important contributing factor to the self-transport behavior of a droplet moving from L to S in an AVGGT is the bridge liquid force caused by negative pressure inside the droplet, which is always pointing in the direction of S. As a result of experiments, we investigated the relationship between droplet motion and correlated parameters. The theoretical model based on the simplified Navier−Stokes equation was developed to explain the corresponding mechanism of the droplet motion. Additionally, dimensional analysis was carried out for the droplet stuck behavior of a droplet moving from S to L in an AVGGT to investigate the relationship between the droplet stopping location and the correlated parameters and thus obtain the required geometry for the droplet stopping location.

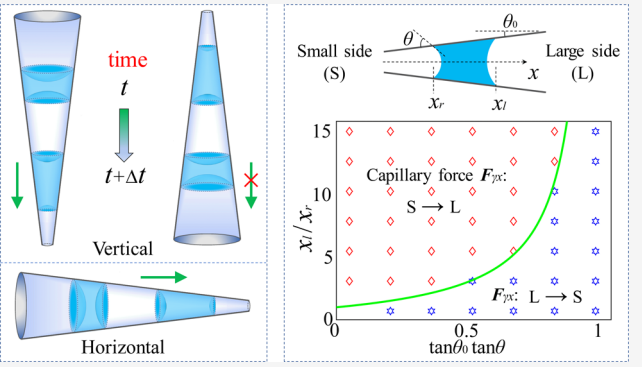

INTRODUCTION

Droplet transport and control have always had potential applications in the fields of industry, medicine, biotechnology, and microfluidics.[1−10] There are some droplet motion phenomena in nature, such as shorebirds feed through their beaks,[11,12] spider silk to directionally collect water,[13] rice leaves with anisotropic sliding properties have the ability to directionally control the movement of water droplets,[14] and water transport on peristome surfaces.[15] Inspired by these natural phenomena, some special structures based on bionics can be used to drive droplet motion.[16−19] According to the previous studies, it can be concluded that one of the key factors to drive droplet motion is the surface structure whose differences mainly derive from materials and geometry. Yin et al.[20−23] conducted extensive research on material differences and prepared different material surfaces using processing techniques such as femtosecond laser, and these different materials give different directional transport effects to droplets. The degree of wetting at the liquid−solid contact interface and the dynamics of the three-phase contact line are important manifestations of how the material affects droplet motion at the macrolevel. Kumar et al.[24] investigated the wetting kinetics of droplets on square micropillar substrates with a radially varying pitch. Gorthi et al.[25] investigated the wetting and contact line dynamics of two immiscible conductive fluids in a narrow fluidic channel under the combined influence of electric and magnetic fields using a diffuse interface-based phase-field model. Randive et al.[26] investigated the contact line dynamics of droplet motion on inclined surfaces with varying wettability characteristics using numerical simulation. Xu et al.[27] used three-dimensional numerical simulations to investigate the dynamics of a self-rewetting drop placed on a substrate with a constant temperature gradient. Droplets in different geometric structures can exhibit different states of motion. Droplet can move spontaneously between two nonparallel plates, and the different opening angles of the wedge formed by the two plates will lead to different movements of the droplet.[28−31] Reyssat[32] proposed a theoretical model to calculate the motion of droplets and bubbles in the wedge formed by two plates. Konda et al.[33] numerically investigated the migration of bubbles in a two-dimensional convergence−divergence channel. Torres[34] has

Received: March 20, 2023
Revised: May 16, 2023
Published: May 26, 2023

https://doi.org/10.1021/acs.langmuir.3c00746
Langmuir 2023, 39, 7901−7911

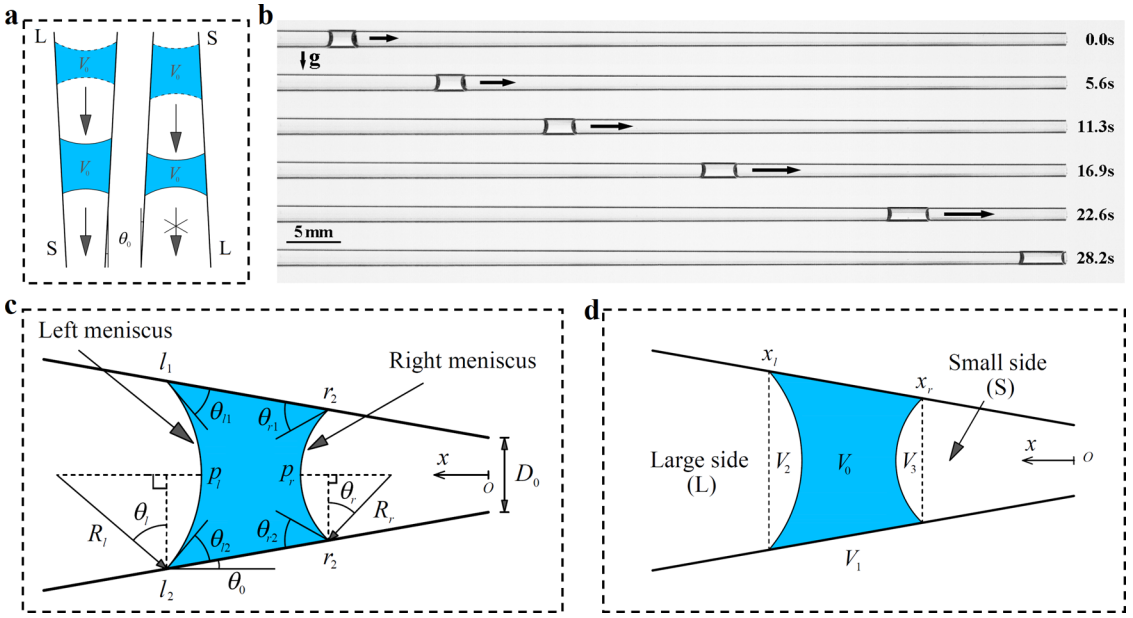

Figure 1. Droplet in the axially varying geometry-gradient tube (AVGGT). (a) Schematic of droplets flowing in different directions with different dynamic behaviors and opposite shape changes. (b) The location of a droplet changes with time in the AVGGT, where the droplet volume is 4 μL and the liquid type is 0.65cs silicone oil; the tube is placed horizontally. (c) Schematic of a droplet placed in the AVGGT (S to point to is defined as the positive direction). (d) Related geometric volumes in the droplet dynamic motion system.

done a lot of work on droplet motion in nonwetting wedges and explored the effects of wedge opening angles, droplet volume, viscosity, etc. on droplet motion. Sen et al.[35] achieved the directional transport of liquid through a geometry-gradient structure with a varying angle. A topological liquid diode is designed to achieve unidirectional flow based on the spontaneous transport of liquids on solid surfaces.[36] Although droplet motion in a nonuniform wedge formed by two plates has been adequately studied, there is a lack of research on droplet motion in nonuniform tubes, and droplet motion in tubes is quite different from that in wedges. There is much research about continuous flow of liquid imbibition in nonuniform tubes. Considering the capillary continuous flow in the tube structure, Young[37] proposed a formulation of the advancing interface in a nonuniform capillary, and the developed formulation can be applied to evaluate the dynamic capillary flow of any other nonuniform capillaries with well-defined geometry. Erickson et al.[38] studied the capillary drive flow in a nonuniform cross section with numerical simulation methods, and they found that the effects of contact angle and surface tension force on the total wetting time were similar to those for straight capillaries. Reyssat et al.[39] established a theoretical model to calculate liquid imbibition in geometries with axial variations. Gorce et al.[40] explored the optimal imbibition of liquids with different curvature tubes. Singh et al.[41] and Iwamatsu[42] presented theoretical investigations of liquid imbibition into capillaries with axially varying geometry, and they found that the conical capillary tube can act as a liquid diode. Michielsen et al.[43] have done extensive theoretical work on droplet motion on the outer surface of conical tubes from an energetic point of view, and their work also takes into account the effects of the droplet volume, contact angle, and angle of change of the tube on droplet self-transport. Recently, Dai et al.[44] fabricated several self-propelled autonomous devices to show the interesting phenomenon of spontaneous motion of droplets in a geometry-gradient structure.

Although tremendous studies have been investigated on the motion of droplets in varying cross-sectional structures (wedge formed by the two plates) and continuous liquid flow in an axially varying geometry-gradient tube (AVGGT), the motion of a single droplet in AVGGT geometries driven solely by capillarity has been less investigated and the effect of liquid bridge force along the flow direction due to tube variations on the motion has been less considered. Droplet motion in an AVGGT is mainly affected by gravity, surface tension force on the three-phase contact line, and liquid bridge force caused by negative pressure inside the droplet, while the latter two forces are closely related to the tube structure, and they constantly change when the droplet moves in an AVGGT. In this study, we use the two forces to explain two dynamic behaviors of the droplet, which are self-transport behavior and stuck behavior, and the droplet motion behaviors are studied by geometric assumption, theoretical analysis, and experimentation. Additionally, the theoretical model based on the simplified Navier–Stokes equation was used to interpret the corresponding mechanism of droplet motion. We want to discuss what factors will affect the droplet motion in the AVGGT, and these factors include the droplet volume, viscosity, density, tube varying angle, and tilt angle. So, this paper focuses on theoretical analysis of droplet motion and generalization of experimental data to obtain the variation of droplet motion with these parameters.

MATERIALS AND METHODS

To better show the change of droplet shape along the axis, we have conducted experiments on the movement of droplets in lyophilic AVGGTs with small varying angles and smaller inner diameters in experiments because liquids cannot form a droplet in larger-diameter tubes (liquid suspends to the walls of the tube, cannot bead up) or the droplet cannot form a symmetrical structure along the axis (the droplet is so large that its shape is strongly influenced by gravity). These tubes exhibit some fascinating liquid diode-like phenomena. The tube is kept upright as indicated in Figure 1a, with the small

https://doi.org/10.1021/acs.langmuir.3c00746
Langmuir 2023, 39, 7901−7911

opening side (S) facing down and the large opening side (L) facing up, and then a droplet is released at L; it will fall downward under the influence of gravity until it reaches the end of the S. On the other hand, if a droplet is released at S with L facing down, the droplet will end up trapped near L. This is due to the droplet deforming, while in motion, its geometrical shape is influenced by the tube geometry, where the shape of droplet varies from "tall and thin" to "short and fat," and the forces acting on the droplet constantly changing, which affects the state of motion. In fact, when the tube is placed horizontally, gravity can be neglected, and the droplets will move spontaneously from L to S.

The fluids used in our experiments are dimethyl silicone oil (Shin-Etsu, KF-96, Japan) and ethanol (Sinopharm Chemical Reagent Co., Ltd., China). We used pipettes (2−20 and 5−50 μL, purchased from China DLAB Distributor) with a needle for liquid injecting. In the experiments of spontaneous movement of droplets from L to S, the tubes are tilted so that the horizontal height of L is lower than S. Then, the droplet is injected from the end of S, and it slides inside due to gravity, eventually stopping on L (droplet can be stuck in the large side, i.e., the stuck behavior), and then slowly the tube is turned to make it horizontal (the center axis of the tube is the horizontal reference line; thus, the effect of gravity is neglected), at which point the droplets start to move spontaneously from L to S, and we film from the lateral side of the tubes to record the movement of the droplets. Additionally, to study the motion of the droplet from S to L, we tilted the tube so that gravity could not be neglected, injected the droplet from the end of S, and measured the distance of the droplets moved at different tilt angles. The results of the experiments are captured with a CCD camera (Hunan Ketianjian Photoelectric Technology Co., Ltd.) at 50 frames per second. The pictures are processed by the gray-scale method (Canny edge detection algorithm[45]), which could provide us with droplet edge coordinates (x_l, x_r) based on different pixel parameters, allowing us to obtain the droplet motion process results.

In our studies, we used AVGGTs made of hyper borosilicate glass, which were purchased from Yancheng Puruiqi Experimental Instruments Co., Ltd. For the axially varying tubes with an invariant gradient, the varying angle θ_0 is 0.175° (as shown in Figure 1a) and the inner diameter D_0 at the small end of the tubes (the tube diameters mentioned in this paper are all inner diameters) is 1.05 mm. Under different levels of wetting, liquid flow would exhibit various dynamic behaviors;[46] the effect of hysteresis on droplet motion can be greatly reduced in this study because all experiments were conducted with pretreatment tubes, which have low hysteresis after prewetting. The pretreatment is that allowing the same liquid (droplet) to move back and forth through in the tube 20 times; then, the tube is left at room temperature for half an hour, and the entire procedure was repeated six times, which resulted in wetting the walls and forming a thin film of liquid; the tube obtained prewetting conditions with low contact angle hysteresis. Bradley et al.[47] demonstrated that this same liquid prewetting method resulted in low contact angle hysteresis, the effect of which is close to the widely accepted slippery liquid-infused porous surfaces (SLIPSs).[48] For the entire droplet system, the droplet densities ρ, kinematic viscosity ν, fluid−air surface tension coefficient γ, and contact angles (liquid-glass) θ (here, we consider equilibrium contact angle as the contact angle, which was obtained by Jurin's height[49]) are given in Table 1 (all measured at temperature T = 25 ± 1 °C).

Table 1. Properties of the Liquid (T = 25 ± 1 °C)

liquid	ρ (kg/m^3)	γ (mN/m)	ν (mm^2/s)	θ (degree)
0.65cs silicone oil	758	15.9	0.65	1.6 ± 0.1
1.0cs silicone oil	816	16.9	1.00	1.6 ± 0.1
2.0cs silicone oil	873	18.3	2.00	1.6 ± 0.2
10.0cs silicone oil	932	20.1	10.00	1.8 ± 0.2
30.0cs silicone oil	952	20.7	30.00	1.9 ± 0.2
100.0cs silicone oil	965	20.1	100.00	2.0 ± 0.1
350.0cs silicone oil	970	20.7	350.00	2.0 ± 0.2
99.7 wt % ethanol solution	790	22.1	1.40	1.7 ± 0.1

RESULTS AND DISCUSSION

Geometric Analysis of Droplets Motion from L to S. A droplet would spontaneously move from L to S of an AVGGT (see Movie S1). To gain a better understanding of the mechanism underlying this droplet motion, the glass tube was initially positioned horizontally in its center axis, where the influence of gravity can be neglected. The droplet shape is constantly changing when it spontaneously moves from the L to the S of an AVGGT (Figure 1b). The schematic of a droplet in an AVGGT is shown in Figure 1c; the left and right menisci of the droplet are marked. The droplet is small enough, and the tube is kept horizontal in its center axis (Figure 1c); thus, we assume that the top and bottom menisci are symmetrical along the tube axis, $l_l \cos\theta_{l1} = l_l \cos\theta_{l2} = l_l \cos\theta$, $l_r \cos\theta_{r1} = l_r \cos\theta_{r2} = l_r \cos\theta$ (θ is the contact angle, subscripts 1 and 2 denote the top and bottom sides of the tube, respectively, l_l and l_r are the contact line lengths). We need to use geometric angles to calculate the radii of the left and right menisci, while the size of the meniscus is related to the tube diameter, so the left and right geometric angles are different because of the change of the tube diameter. When the droplet moves from L to S, the left meniscus is a receding interface; thus, the left geometric angle (Figure 1c) $\theta_l = \theta_{re} + \theta_0$. Additionally, here, we assume that the receding contact angle θ_{re} is the same as the contact angle θ; thus, the left geometric angle θ_l is given by

$$\theta_l = \theta + \theta_0 \tag{1}$$

For liquid flow in capillary tubes, we can know from the Hoffman curve[50] that the dynamic advancing contact angle θ_{ad} depends on the capillary number (Ca = $\rho\nu u/\gamma$, where u is the droplet velocity). An empirical equation found by Remmortere[51] applies to the advancing angle of silicone oil in glass capillaries; it is

$$\cos\theta_{ad} = \cos\theta - 2(1 + \cos\theta)\mathrm{Ca}^{1/2} \tag{2}$$

Therefore, the right geometric angle is given by (when $\theta_{ad} > \theta_0$)

$$\theta_r = \theta_{ad} - \theta_0 \tag{3}$$

According to the Young−Laplace equation,[49] the internal pressure in the meniscus on both sides of the droplet is given by

$$p_i = \frac{-4\gamma\cos\theta_i}{D_i} (i = l, r) \tag{4}$$

where $D_i = D_0 + 2x_i \tan\theta_0$ ($i = l, r$) is the diameter of the tube on the three-phase contact line of the droplet. Due to the irregular shape of a droplet located in the AVGGT, the droplet cannot be seen as a particle in mechanical analysis; thus, we confirm the mass center position (x_0) of the droplet according to geometric calculation. As shown in Figure 1d, we use V_0, V_1, V_2, and V_3 to denote the relevant volumes, respectively. V_0 is the droplet volume, V_1 is the circular truncated cone volume made up of the lateral edge of the droplet and the bases of menisci, V_2 is the volume of the left spherical segment, and V_3 is the volume of the right spherical segment (the concave meniscus and base of the circular truncated cone make up the spherical segment). We assume that, in the case of the small

https://doi.org/10.1021/acs.langmuir.3c00746
Langmuir 2023, 39, 7901−7911

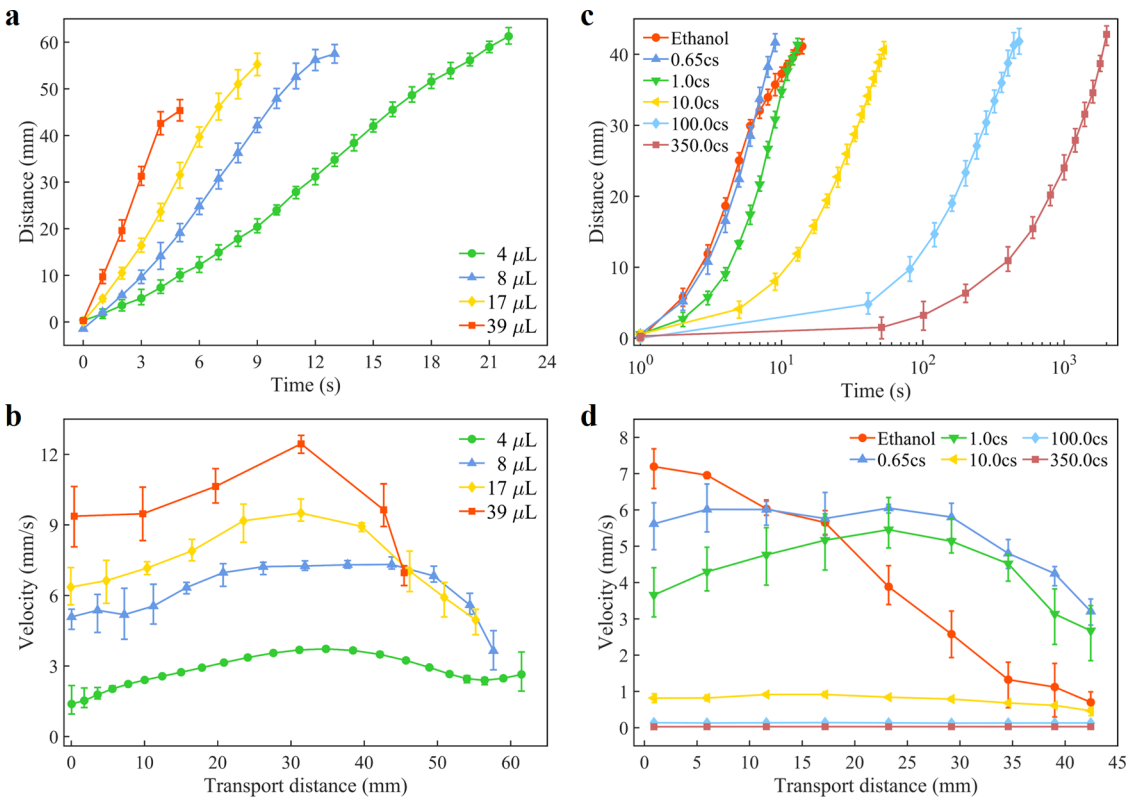

Figure 2. Analysis of the droplet motion process: (a) transport distance versus time for 0.65cs silicone oil droplets at different volumes. (b) Velocity versus time for 0.65cs silicone oil droplets at different volumes. (c) Transport distance versus time for 10 μL droplets at different viscosities (fluids). (d) Velocity versus time for 10 μL droplet at different viscosities (fluids).

droplet volume, several geometries are symmetric along the central axis of the tube. Then, we calculated the error of geometric length (relevant radius, width and height of spherical segment) between these geometric assumptions and experimental measurements; the error is less than 0.4 mm, and finally, we can get the result of $x_0(t)$ as a function of time t according to the geometric calculation. The relevant geometric calculations are shown in S1 of the Supporting Material (SM).

Analysis of the Droplet Motion Process. Through experiments, we can obtain the motion of different volumes of droplets (Movie S2); the data of droplet motion can be got by processing these movies, and the displacement formula $x_0(t)$ of droplet can be got by fitting these data (Figure 2a); then, we can know that the larger the volume of the droplet, the faster it moves. The velocity of the droplet can be deduced from the displacement formula $x_0(t)$; it is given by $u(t) = dx_0/dt$. Then, we reconstructed the relationship between velocity and displacement, and the results are shown in Figure 2b; we can know from the results that, when the droplet gets closer to the S terminal, its velocity increases. Additionally, we are interested in how the droplet moves when the other parameters of the liquid change; thus, the silicone oils of 0.65cs, 1.0cs, and 10.0cs and ethanol are used in experiments (Movie S3). A droplet motion tendency can be found that the droplets would move more slowly when the liquid viscosity is larger, while for ethanol, it has a larger surface tension coefficient, and the attenuation of motion is more intense than for silicone oil (Figure 2c,d). Note that different liquid viscosities mean different types of silicone oil in this paper because for a wide range of viscosity changes, the viscosity cannot be changed independently without changing other physical properties as shown in Table 1.

From Figure 2b,d, we can see that the velocity of droplets decreases as they approach the small side end of the tubes. In fact, when droplet moves inside the tube, the advancing meniscus of the droplet has an effect on the liquid film in front of it and this liquid film is shifted.[52,53] Additionally, according to the Gibbs criterion[54] and the work of Hyun et al.,[55] liquid cannot pass over the end edge until its contact angle θ exceeds the critical value θ_{cr}. Therefore, the motion of the liquid film is stalled by the edge of the small side end, which affects the droplet motion, and the droplet is decelerated near the end edge. The droplet even rebound vibration when it reaches the S terminal, like a water hammer, as illustrated in Movie S2, it is obvious for the volumes with 17 and 39 μL. Here, we do not explain this phenomenon much; our focus is on the motion of droplets in AVGGTs.

Force Analysis of the Droplet Motion. As shown in Figure 1b, when a droplet moves from L to S, the length of the droplet transform from "short" to "long", and the forces acting on the droplet will constantly change in the movement process. As the droplet flows from S to L in AVGGTs, the droplet seems to be stretched longitudinally as the diameter of the tube becomes larger and larger, and this stretch is caused by the liquid bridge force that is generated by the negative pressure on the droplet and the contact wall.[28] For a droplet in an AVGGT, the liquid bridge force caused by the negative pressure inside the droplet has a component in the axial direction, which acts together with the axial surface tension on the three-phase contact line, allowing the droplet to flow spontaneously from L to S. We conducted a more detailed

https://doi.org/10.1021/acs.langmuir.3c00746
Langmuir 2023, 39, 7901−7911

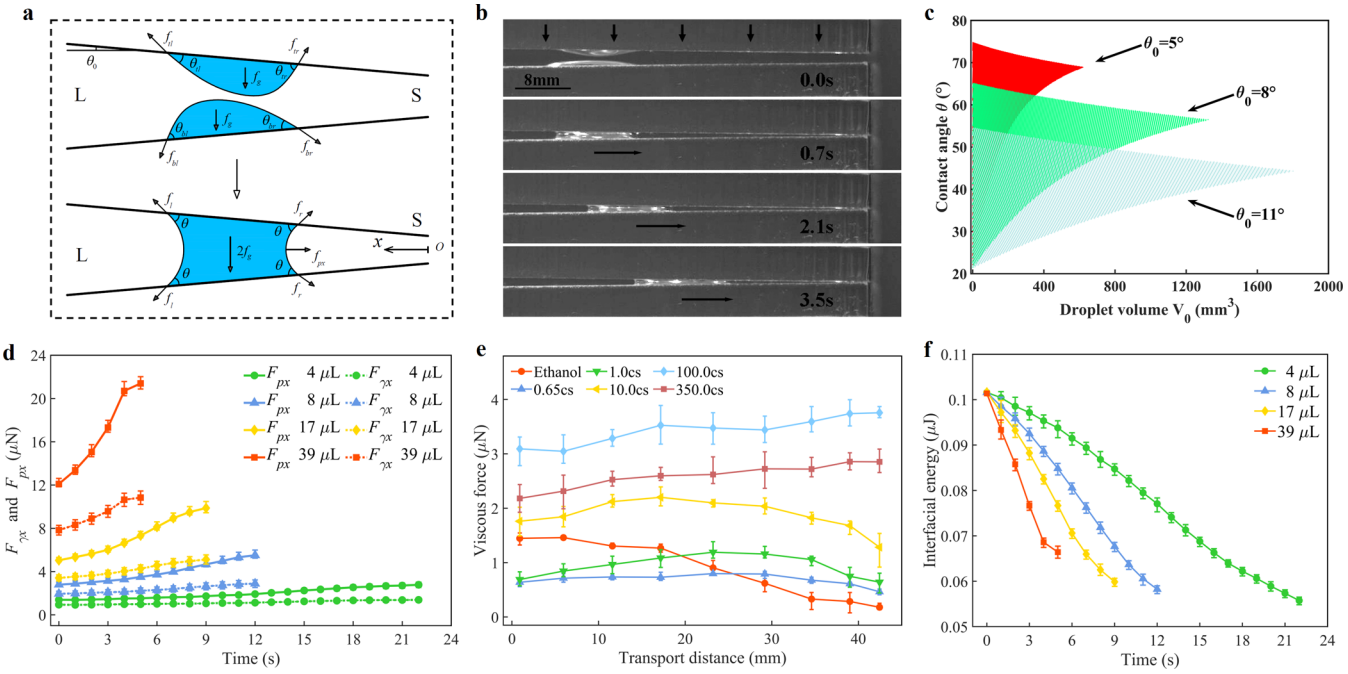

Figure 3. Force and energy analysis of the droplet motion: (a) schematic of the forces on the droplets before and after merging. (b) Spontaneous motion of the formed droplet (70 wt % ethanol solution). (c) Results of $f < 1$ for different geometric parameters. (d) Results (0.65cs silicone oil droplet at different volumes) of the surface tension force (opposite to the flow direction) and the liquid bridge force (along the flow direction) in the x direction change with time, where the dotted and solid lines are the surface tension force and the liquid bridge force, respectively. (e) Viscous force versus transport displacement for different types (viscosity) of 10 μL droplets. (f) Interfacial energy of the 0.65cs silicone oil droplet at different volumes change with time.

force analysis for the two forces in S2 of the SM. It is worth noting that, in this study and subsequent expressions, the force in the x direction at the liquid−solid contact surface due to the negative pressure inside the droplet is referred to as the liquid bridge force F_{px}, and the force in the x direction derived from the Laplace stress on the liquid−gas contact surface is referred to as the surface tension force acting on the three-phase line $F_{\gamma x}$.

Here, we did analysis about these horizontal forces, considering a two-dimensional model; two identical small droplets, respectively, remain stationary at the top edge and bottom edge as shown in Figure 3a. For the top and bottom two individual droplets that have not yet merged, in the direction parallel to the wall, the surface tension forces between the left and right sides of the two droplets are in equilibrium with gravity (the forces perpendicular to the wall are not considered). We assume that the apparent contact angles (in fact, their contact angles are the same, but the apparent contact angles are different and then will cause a change in the shape of the menisci of the droplet and thus in its Laplace pressure[49]) $\theta_{tl} = \theta_{br} = \theta_1$, $\theta_{tr} = \theta_{bl} = \theta_2$ (in the previous section we assumed that the top and bottom droplets have the same shape); thus, the surface tension forces $f_{tl} = f_{br} = f_1$, $f_{tr} = f_{bl} = f_2$, and these surface tension forces are related to the length of the contact line on both sides. This assumption is mainly to demonstrate that when the volume of the droplet is very small, the effects of gravity on its shape are small, i.e., two droplets remain in an antisymmetric shape along the axis of the tube. Since the two droplets are at rest, their resultant forces in the direction parallel to the top and bottom edges, respectively, are both zero, and the relations of the forces are given by

$$f_1 \cos\theta_1 = f_g \sin\theta_0 + f_2 \cos\theta_2 (\text{top}) \tag{5}$$

$$f_2 \cos\theta_2 + f_g \sin\theta_0 = f_1 \cos\theta_1 (\text{bottom}) \tag{6}$$

If the droplets are placed further to the right, i.e., the distance between the top and bottom sides become smaller, the top droplet will eventually touch the bottom droplet and merge into a larger droplet. At that moment of contact, there will be a new force f_a (liquid−liquid attraction) acting on the top and bottom droplets, respectively, which is perpendicular to the wall of the tube and points to the other droplet (note that the inclination of the wall remains unchanged despite the tube narrowing and the force condition of the droplet will remain unchanged prior to touching). The liquid−gas (droplet−air) attractions of top and bottom droplets are negligible during the total touch process because they are much smaller than the liquid−liquid (top−bottom droplet) attraction. Therefore, at that moment of contact, in the direction parallel to the top and bottom walls, respectively, the two droplets will each have a new force condition, which are

$$f_1 \cos\theta_1 < f_g \sin\theta_0 + f_2 \cos\theta_2 + f_a \tag{7}$$

$$f_2 \cos\theta_2 + f_g \sin\theta_0 - f_a < f_1 \cos\theta_1 \tag{8}$$

The right-hand side of the above two equations is both larger than the left-hand side, so the new merged droplet spontaneously moves toward right. For the merged droplet, a new force condition is established in the x direction, which is

$$2f_l \cos\theta \cos\theta_0 < 2f_r \cos\theta \cos\theta_0 + f_{px} \tag{9}$$

where the liquid bridge force f_{px} in the direction of x acts as the driving force for the droplet; we do not consider the viscosity force here first. The liquid bridge force acts on the contact interface of the liquid-wall, which is caused by the negative

https://doi.org/10.1021/acs.langmuir.3c00746
Langmuir 2023, 39, 7901−7911

pressure inside the droplet (liquid−liquid attraction is weaker than liquid−solid attraction). Here, we use two acrylic plates to show this phenomenon; two droplets stay on the top and bottom plates, respectively. The top plate is pushed down (in the vertical direction), and the two droplets are made to contact with each other; then, the new formed droplet will move spontaneously from the left to the right, as shown in Figure 3b and Movie S4. It is worth noting that different liquids are used for the top and bottom plates (for example, water for the top plate and ethanol for the bottom plate), the spontaneous movement of the droplets after merging can also occur when the ratio between them is appropriate. Although this experiment is a three-dimensional situation for our contact hypothesis, it largely supports the two-dimensional model. However, the change of the shape and force of the droplets at the instant of contact between the top and bottom droplets are very complex, so here we only explore the force states before and after the droplet contact.

The resultant force acting on a droplet in the direction of the x axis is (S toward L is the positive direction of the x axis)

$$F = F_v + F_{\gamma x} - F_{px} \tag{10}$$

where $F_{\gamma x}$ is the x component of the total surface tension force between the left and right three-phase contact lines of droplet, F_{px} is the x component of the liquid bridge force caused by negative pressure in the droplet, and F_v is the viscous force in the contact area (droplet-wall). The surface tension force component $F_{\gamma x}$ can be calculated[40] as follows,

$$F_{\gamma x} = \pi\gamma(D_l \cos\theta_l - D_r \cos\theta_r) \tag{11}$$

At first, we think that the surface tension force at right ($\pi\gamma D_r \cos\theta_r$) is greater than that at left ($\pi\gamma D_l \cos\theta_l$) (because of the varying angle, $\cos\theta_l < \cos\theta_r$, Figure 1c), so the total surface tension force acts as a driving force. However, the effect of the varying angle makes the circumference of the contact line longer ($D_l > D_r$) in our experiments, which leads to $D_l \cos\theta_l > D_r \cos\theta_r$, so that the total surface tension force is not the driving force in the spontaneous motion. In fact, the surface tension force can also be a driving force under different conditions, for which we define f as a parameter to discuss the role of surface tension on the droplet.

$$f = \frac{D_l \cos\theta_l}{D_r \cos\theta_r} \tag{12}$$

If $f < 1$, the surface tension force can be a driving force for the droplet motion from L to S (i.e., spontaneous motion); thus, we use f as a criterion to determine the surface tension force whether it can be seen as the driving force to act on a droplet spontaneously moving from L to S in an AVGGT. In fact, their relationship depends on four basic parameters (see Figure S3), position parameters x_r and x_l, contact angle θ, and tube varying angle θ_0; thus, we obtained the function $f(x_r, x_l, \theta, \theta_0)$. Some numerical calculations were performed for compare the magnitudes of f and 1. For these calculations, first, let x_r = 30 mm (it is arbitrary, but it can reflect some of the laws we seek in our research), a calculation range (x_r−x_r + 50 mm, interval is 0.1 mm) for x_l and a range (1−90°, interval is 0.5°) for contact angle θ are chosen. Then, we substituted all different parameter points of these ranges into the function f (at three constant varying angles θ_0 5°, 8°, 11°, respectively) to obtain the results for $f < 1$; the specific computational procedure and the larger computational range of the calculations can be seen in S3 of the SM. Finally, we marked these results ($f < 1$) with several colors different from the background color (white, $f > 1$), and the x_l can be expressed in terms of V_0 by the previous geometric relations, so we obtained the relationship between the droplet volume and the contact angle when the other two parameters are fixed; the results are shown in Figure 3c.

To calculate the liquid bridge force component inside the droplet, we assume that the pressure distribution along the wall inside the droplet is linear, which holds because the volume of the droplet is small and the tube varying angle (influences the meniscus radii at both sides of the droplet) is also small. Thus, the pressure distribution in the interface between the droplet and the tube wall is given by

$$p = p_r + \frac{p_l - p_r}{\Delta X}(x - x_r) \tag{13}$$

where $\Delta X = x_l - x_r$ is the length of the droplet.

Subsequently, the x component of the liquid bridge force is the pressure integrated over the circular truncated cone lateral area (wall-droplet contact area)

$$\begin{aligned} F_{px} &= \sin\theta_0 \int_{x_r}^{x_l} \pi p D(x)\mathrm{d}x \\ &= \frac{\pi \sin\theta_0 \Delta X}{6}[3D_0 p_i + 2\tan\theta_0(p_i x_j + \delta_{ij} p_i x_j)] \end{aligned} \tag{14}$$

where the result is a tensor, with i, j = r, l, and δ_{ij} is the Kronecker symbol.

The change of the surface tension force and liquid bridge force over time is illustrated in Figure 3d. The results show that they both increase with time; the liquid bridge force increases faster than the surface tension force, so the difference between the two forces gradually increases. As a result, the droplets move faster and faster with time (liquid bridge force acts as a driving force). In essence, the increase of the two forces is caused by the tube structure, which makes the droplet change from "short and fat" to "tall and thin". The increase of the surface tension force is due to the increase in the length of the droplet, and the difference between the diameters of the two sides of the droplet becomes larger and larger. Meanwhile, the increase of the liquid bridge force is due to the increase in contact area between the liquid and the tube wall. Therefore, as the droplet moves from L to S, its resultant force increases, causing the droplet to accelerate. However, as the droplet approaches the end of S of the tube, its velocity begins to decrease due to interference from the boundary; however, this boundary effect is not the focus of our work, which instead focuses on the motion law of the droplet in the tube.

To calculate the viscous force, the simplified Navier−Stokes equation based on our model is given by

$$\frac{\mathrm{d}p}{\mathrm{d}x} = \frac{\mu}{r}\frac{\partial}{\partial r}\left(r\frac{\partial u_x}{\partial r}\right) \tag{15}$$

where the origin is the intersection of the S end edge and the tube axis, x is parallel to the axis and points from the origin to the L side, r is perpendicular to the axis and points to the tube wall, $\mu = \rho\nu$ is the dynamic viscosity, and u_x is the velocity of the droplet along the x direction, and the equation is solved using the no-slip boundary condition $u = 0$ at $r = \pm D(x)/2$ and $\mathrm{d}u/\mathrm{d}r = 0$ at $r = 0$, which gives

https://doi.org/10.1021/acs.langmuir.3c00746
Langmuir 2023, 39, 7901−7911

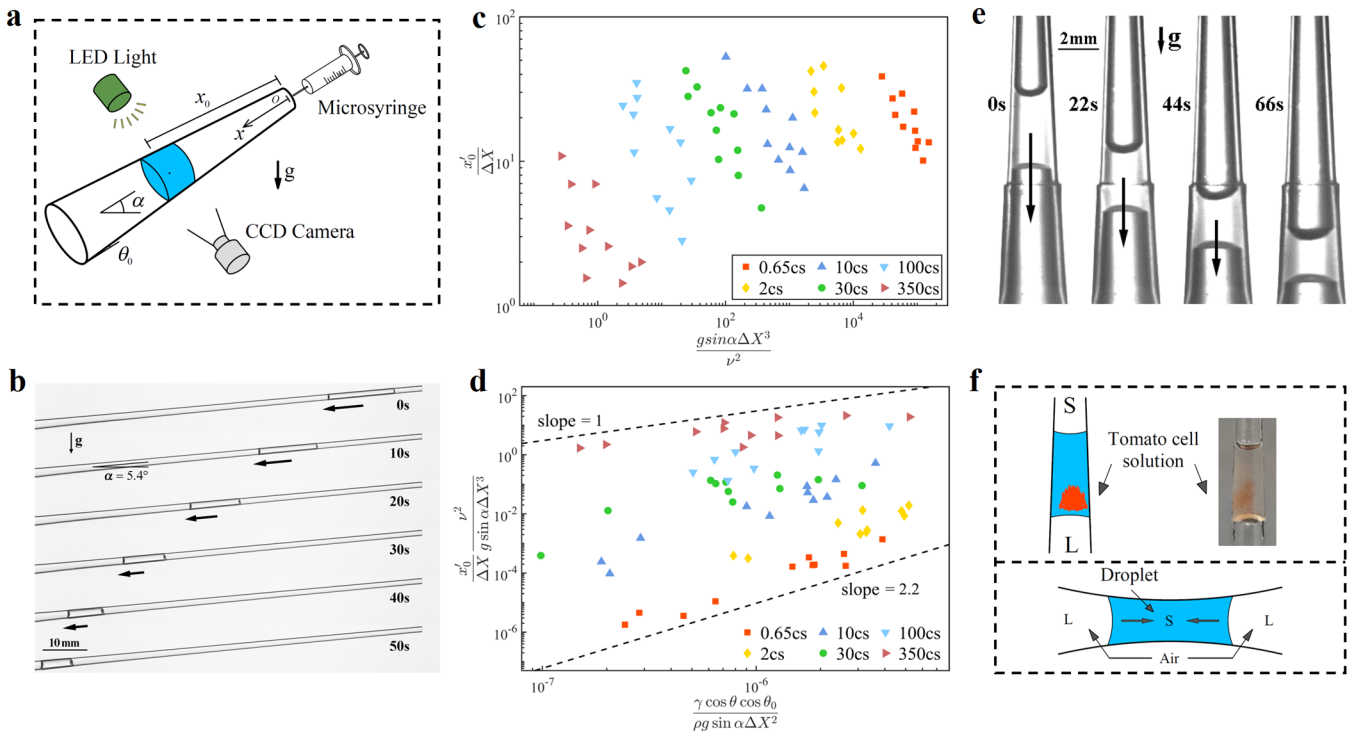

Figure 4. Droplets moving from S to L under gravity. (a) Schematic of the experimental system for the droplet motion in a tilt AVGGT. (b) Distance results of a 15 μL droplet with 10cs silicone oil and 5.4° tilt angle. (c) Separate trends between π_1 and π_2. (d) Collapse of experiment data according to the scale analysis. (e) A 6 μL droplet in a vertical AVGGT with varying angle 2.9°. (f) Top: tomato cell solution storage; bottom: schematic of a droplet storage in a tube, which has a small diameter at the middle and a large diameter at the sides.

$$u_x = \frac{4r^2 - D(x)^2}{16\mu}\frac{\mathrm{d}p}{\mathrm{d}x} \tag{16}$$

where the tube diameter in the edge of the droplet $D(x) = D_0 + 2x\tan\theta_0$. To better calculate the relevant motion of the droplet, we use the average flow rate instead of the varying flow rate, which is expressed as

$$\overline{u}_x = \frac{4}{\pi D(x)^2}\int_0^{D(x)/2} 2\pi r u_x \mathrm{d}r = -\frac{D(x)^2}{32\mu}\frac{\mathrm{d}p}{\mathrm{d}x} \tag{17}$$

Then, we can get the pressure gradient

$$\frac{\mathrm{d}p}{\mathrm{d}x} = -\frac{32\mu\overline{u}_x}{D(x)^2} \tag{18}$$

The Laplace pressures across the left and right liquid−air interfaces are given by the Young−Laplace equation, which are expressed as

$$p_a - p_l = \frac{4\gamma\cos(\theta + \theta_0)}{D(x)} \tag{19}$$

$$p_a - p_r = \frac{4\gamma\cos(\theta - \theta_0)}{D(x)} \tag{20}$$

where p_a is the atmospheric pressure. The droplet length $\Delta X = x_l - x_r$ has a small change with the displacement, and the slope of the tube is constant; thus, we assume that the length varies linearly with the displacement. Then, we get the droplet length $\Delta X(x)$ based on our tube parameter and experimental data, it is expressed as $\Delta X = X_{\max} - Ax/L$,where L is the total displacement of the droplet, $A = X_{\max} - X_{\min}$, where $X_{\max}$ and $X_{\min}$ are the maximal and minimum lengths of the droplet during the entire motion, respectively.

Then, we can obtain the pressure gradient

$$\frac{\mathrm{d}p}{\mathrm{d}x} \approx \frac{p_r - p_l}{\Delta X} = -\frac{8\gamma\sin\theta\sin\theta_0}{D_0 + 2x\tan\theta_0}\frac{L}{LX_{\max} - Ax} \tag{21}$$

Using eq 21 in eq 16 gives

$$u_x \approx \frac{D(x)^2 - 4r^2}{2\mu}\frac{\gamma\sin\theta\sin\theta_0}{D(x)}\frac{L}{LX_{\max} - Ax} \tag{22}$$

Using eq 21 in eq 17 gives

$$\overline{u}_x \approx \frac{\gamma D(x)\sin\theta\sin\theta_0}{4\mu}\frac{L}{LX_{\max} - Ax} \tag{23}$$

Then, the velocity gradient is given by

$$\frac{\mathrm{d}u_x}{\mathrm{d}r} = \frac{r}{2\mu}\frac{\mathrm{d}p}{\mathrm{d}x} = -\frac{16\overline{u}_x r}{D(x)^2} \tag{24}$$

Consequently, the viscous stress at the tube is

$$\tau = \mu\left|\frac{\mathrm{d}u_x}{\mathrm{d}r}\left(\pm\frac{D(x)}{2}\right)\right| = \frac{8\mu\overline{u}_x}{D(x)} \tag{25}$$

The total viscous force of the tube on the droplet is the viscous stress integrated over the solid−liquid contact areas, and its component in the x direction is

https://doi.org/10.1021/acs.langmuir.3c00746
Langmuir 2023, 39, 7901−7911

$$F_{vx} = \cos\theta_0 \int_{x_r}^{x_l} \pi\tau \frac{(D_l + D_r)}{2} \frac{\mathrm{d}x}{\cos\theta_0} \approx 8\pi\mu\overline{u}_x \Delta X \left[1 + \frac{X_{\max}\tan\theta_0}{D_0 + 2x\tan\theta_0}\right] \quad (26)$$

The change of the viscous force over transport distance is illustrated in Figure 3e; the results show that the higher the viscosity of the liquid, the larger the viscous force acting on the droplet transport process. However, when the viscosity is too high (350cs), it can be found that the calculated viscous force is less than that of the droplet at lower viscosity (100cs), which is because the velocity of 350cs silicone oil is much lower than 100cs.

Energy Analysis of the Droplet Motion. The energy E of the entire droplet system consists of gravity potential energy E_g, kinetic energy E_v, interfacial energy E_γ, and dissipation Φ. The formula for the total energy is $E = E_g + E_v + E_\gamma + \Phi$. For the tube that is positioned horizontally, the gravity potential energy is zero (the center axis of the tube is used as the horizontal reference line). The kinetic energy is $E_v = mu_x^2/2$; it varies with velocity. The liquid−solid contact area of the entire tube system remains constant since the tube is prewetted; the inner wall of the tube has a liquid film on it, and the droplet does not directly contact the wall. Consequently, we can consider that there is no liquid−solid interfacial energy exchange in the whole motion system, and the total liquid−liquid interfacial energy is constant, so there is only the interfacial energy change of liquid−gas. The change of interfacial energy for a single droplet has only the interfacial energy of the droplet−air interface $E_\gamma = \gamma(S_l + S_r)$, where S_l and S_r are the left and right droplet−air contact areas, respectively. When we start to release a droplet at L, the droplet−air areas decrease as the droplet moves from L to S, i.e., the interfacial energy of the droplet starts to decrease, while the kinetic energy increases and the velocity increases. The viscous dissipation inside the droplet during droplet movement is challenging to calculate, but since it is not the primary focus in this study, we do not calculate it here. The results of interfacial energy changing with time for different droplet volumes (Figure 3f) show that the larger the droplet volume, the faster the change of interfacial energy, and the energy is converted into kinetic energy and dissipation energy. This can be considered as a verification from the energy point of view that the larger the droplet volume, the faster the droplet moves.

Droplets Moving from S to L under Gravity. The work mentioned above suggests that the unbalanced forces acting on the droplets are what causes the phenomenon, whereby droplets move spontaneously from L to S in an AVGGT. The gravity will act along the axis and cause the droplet to move from S to L when the tube is tilted. In experiments, the AVGGT is tilted at a certain angle α, while the tube is kept fixed, and a droplet is subsequently injected at the end of S. The droplet then flows toward L and stops at a certain location, where the distance of the mass center of the droplet to the origin of coordinates O is denoted as x_0 (Figure 4a). We conducted experiments in the AVGGTs by altering the droplet volume, liquid viscosity, surface tension coefficient, density, and tilt angle (different tilt angles will lead to the different gravity force components of the droplet in the direction of movement) to investigate the factors related to the final stopping location x_0' of the droplet. Based on the known tube structure and the obtained stopping location x_0', we can calculate the shape of the droplet at stagnation as well as the geometrical constraints it is subjected to, and finally, we can determine the conditions required for the droplet to be stuck in the tube, which can provide some reference significance for droplet storage in variable cross-sectional tubes.

The shape of a droplet changes from "tall and thin" to "short and fat" as it moves from S to L (Figure 4b), and its force condition also changes as it moves toward the larger side. Note that when a droplet moves in a nonhorizontal tube, the bottom interface of the droplet will be flattened, which is caused by the gravity. Consequently, there are different apparent contact angles (different menisci structures) for the two sides, θ_t and θ_b (top side and bottom side), which change with the gravity (different gravities of droplets along axis of tubes are due to the different tilt angles α). The meniscus of the bottom side becomes more and more flatter with the increase of the droplet gravity;[49,51] thus, the apparent contact angle of bottom side θ_b becomes larger and larger. In addition, the "flatten effect" increases as the tube diameter increases (curvature of the meniscus decrease). Therefore, the capillary force of the bottom side will reduce because of the decrease of $\cos\theta_b$ (it leads to an increase in the radius of the bottom meniscus and a decrease in capillary pressure). The new resultant force acting on the droplet is

$$F = F_g \sin\alpha + F_{\gamma x} - F_{px} - F_v \quad (27)$$

$$F_{\gamma x} = \pi\gamma(D_b\cos\theta_b - D_t\cos\theta_t) \quad (28)$$

For the droplet motion from L to S, $F_{\gamma x}$ is opposite to the flow direction (with the experimental setting), but it is along the flow direction in the motion from S to L. This is because the bottom apparent contact angle becomes larger compared with the unchanging top apparent contact angle, i.e., the curvature of the meniscus becomes smaller, $D_b\cos\theta_b < D_t\cos\theta_t$. In addition, the liquid bridge force F_{px} is also affected by the bottom apparent contact angle θ_b. Hence, the resultant of surface tension force and liquid bridge force will increase when the droplet moving to the large side, and then the droplet stops in a location and achieves a force balance condition.

It is difficult to measure the bottom apparent contact angle after flattening in the experiments per frame (measuring the apparent contact angle needs to magnify the picture and provides a different light source environment); thus, here we only explore which parameters are related to the mass center x_0' of the droplet stopping location, and these parameters are the droplet density ρ, length ΔX, kinematic viscosity ν, volume V_0, contact angle θ, surface tension coefficient γ, tube varying angle θ_0, and tilt angle α. Then, we can obtain these parameters as a function of the dimension analysis; the function is

$$x'_0 = f_1(\Delta X, \nu, \rho, \gamma, V_0, g, \alpha, \theta, \theta_0) \quad (29)$$

In fact, the droplet's volume remains constant throughout motion and has a purely geometric relationship with geometric factors such as the droplet's length and location (i.e., the geometry of the tube), that is $V_0 = V_0(x_0, \Delta x, \theta, \theta_0)$, and the relevant calculation results are detailed in S3 of the SM. Then, we can simplify the dimension analysis calculations by reducing the volume variables since it is not a completely independent variable. It is worth noting that we batch produced AVGGTs only for one varying angle ($\theta_0 = 0.175°$), and the contact angle of the liquid used in our experiments varies very little ($\theta = 1-$

https://doi.org/10.1021/acs.langmuir.3c00746
Langmuir 2023, 39, 7901−7911

3°); here, we assume it is 2°, and thus, the two angles can be considered as constants in our experiments, and they are only considered in the analysis during the geometry and force calculations. Additionally, by analyzing the relevant calculation equations, two gravity factors can be combined ($g\sin\alpha$) and surface tension force can be simplified to that $\gamma\cos(\theta \pm \theta_0) \approx \gamma\cos\theta\cos\theta_0$, by $\sin\theta\sin\theta \ll \cos\theta\cos\theta_0$; then, the new function relationship is

$$x'_0 = f_2(\Delta X, \nu, \rho, g\sin\alpha, \gamma\cos\theta\cos\theta_0) \tag{30}$$

We conducted experiments with various parameters to collect data for analyzing the motion of the droplet from S to L. In the experiments, the droplets are all released at the S end of the tube with zero initial velocity. Some droplet initial positions are slightly farther from the end, but no more than 5% of the total distance, so we assume that they are released at the end (origin) to simplify the calculation. Different factors cause differences in the droplet motion and eventual stopping location, which are shown in Movies S5 (15 μL volume in an AVGGT at tilt angles 2.3, 3.4 and 5.4°) and S6 (4 μL droplet volume in an AVGGT at tilt angles 9.3 and 12.1°). From a preliminary calculation of our experimental data, we can determine that the Weber number $We = \rho u^2 D/\gamma$ of the droplet is very small, falling between 10^{-4} and 10^{-2}, so that we can neglect the inertial force of the droplet compared to the surface tension, which allows us to assume that the final stopping location of the droplet is independent of its velocity. Different types of silicone oil have different physical properties as shown in Table 1 and one parameter that does not change independently with the change of oil type. For different silicone oil, there are different results in experiments, and in order to show the relations between these parameters, we did dimensionless analysis based on the Buckingham Pi theorem.[56] The dimensionless analysis method shows that the droplet final stopping location is determined by three dimensionless parameters π_1, π_2, and π_3, and their expressions are given by

$$\pi_1 = \frac{x'_0}{\Delta X} \tag{31}$$

$$\pi_2 = \frac{\nu^2}{g\sin\alpha\Delta X^3} \tag{32}$$

$$\pi_3 = \frac{\gamma\cos\theta\cos\theta_0}{\rho g\sin\alpha\Delta X^2} \tag{33}$$

Then, eq 30 can be changed into

$$\frac{x'_0}{\Delta X} = f_3\left(\frac{\nu^2}{g\sin\alpha\Delta X^3}, \frac{\gamma\cos\theta\cos\theta_0}{\rho g\sin\alpha\Delta X^2}\right) \tag{34}$$

According to our experimental results, we can know that π_1 and π_2 have a negative correlation (Figure 4c), and then we try to construct a new functional relationship

$$\frac{x'_0}{\Delta X}\frac{\nu^2}{g\sin\alpha\ \Delta X^3} = f_4\left(\frac{\gamma\cos\theta\cos\theta_0}{\rho g\sin\alpha\Delta X^2}\right) \tag{35}$$

Then, we can get the collapse of experimental data according to eq 35, as shown in Figure 4d, and by processing these results, we can obtain a further expression

$$x'_0 = \frac{k\rho(\gamma\cos\theta\cos\theta_0)^n}{\mu^2(g\sin\alpha)^{n-1}\Delta X^{2(n-2)}} \tag{36}$$

where k and n (1−2.2) are constants determined by experiments and $\mu = \rho\nu$ is the dynamic viscosity. So, based on the previous geometric assumptions, we can calculate what the tube parameters are when the droplet is stuck in the location x_0' and use them to design the corresponding liquid storage device.

We can use the clogging phenomenon to store droplets. Figure 4e shows that a silicon oil droplet moves from S to L in a vertical polyethylene tube (tilt angle α is 90°), and the droplet finally rests on the side of the tube near L. AVGGT-like structures are common in scientific research, such as conical tips of pipette guns and glass drippers. For a smart pushing irrigation device (e.g., drip irrigation technology in water-scarce areas, with one pipette gun per plant), if the force provided by the pushing device and the time to apply the force are constant (consuming as little energy as possible) and when the output tube of the device is an AVGGT, either the droplets inside the tube need more energy to push them out of the tube due to clogging phenomenon or need less energy due to the spontaneous phenomenon. For a biotechnological flow experiment, we can leave the AVGGT in the experimental channel, and when we need to save certain cell solution (Figure 4f top diagram) or liquid for a short time during the experiments, we can let the droplet (liquid) flow to the AVGGT present in the experimental setup and take the tube directly down with the droplet (because of AVGGT's stagnation phenomenon, the droplet will not flow out), seal it, and freeze it rather than placing the droplet in a new container, which would increase contamination. Then, when the liquid is required again, the tube can be reinserted into the experimental setup and the liquid is unfreezed. A tube can be designed (Figure 4f bottom diagram), which has a small diameter at the middle and large diameter at the outside. It can reserve a droplet in the middle of the tube, where the droplet can steadily stay in the middle of the tube without external interference, and an experiment was also conducted in this tube (Movie S7).

CONCLUSIONS

In this work, we analyzed two dynamic processes (two travel directions, L to S and S to L) of a droplet moving in the AVGGT. The mechanism of the droplet motion is explored based on the geometric assumption and mechanical analysis by considering the droplet volume and liquid type. In detail, the surface tension force and bridge liquid force are used to explain the droplet dynamic behaviors and spontaneous and clogging phenomena. Depending on the tube structure, surface tension can act as driving or impeding force, and we explored the conditions under which surface tension acts as driving or impeding force by numerical calculations. For droplet motion from L to S, we qualitatively proposed a model to interpret the self-transport phenomenon and demonstrate the model by experiment. The bridge liquid force is always the driving force for droplets moving from L to S, inducing the self-transport behavior. Based on the simplified Navier−Stokes equation, we calculated the velocity profile of a droplet moving from L to S in an AVGGT and concluded from the experimental results and theoretical analysis that the droplet velocity increases with the increase of droplet volume and decreases with the increase of droplet viscosity. We verified these conclusions of droplet

https://doi.org/10.1021/acs.langmuir.3c00746
Langmuir 2023, 39, 7901−7911

self-transport from the force and energy point of view. Finally, we used dimensionless analysis to quantitatively generalize the droplet final stopping location in the AVGGT as the droplet moves from S to L, obtained relationships between the droplet stopping location and correlated parameters, and proposed relevant application of droplet storage based on the clogging phenomenon.

■ ASSOCIATED CONTENT

Supporting Information

The Supporting Information is available free of charge at https://pubs.acs.org/doi/10.1021/acs.langmuir.3c00746.

Droplet movement in the AVGGTs (Supporting Material) (PDF)

Droplets flow from L to S in the AVGGT (Movie S1); droplets flow from L to S in the AVGGTs in different volumes, 4, 8, 17, and 39 μL (Movie S2); different types (0.65cs, 1.0cs, 10.0cs silicone oil and ethanol) of droplets flow from L to S in the AVGGTs (Movie S3); spontaneous movement of the droplet formed by droplets (70% wt ethanol solution) from the top and bottom plates (Movie S4); 15 μL droplets (10cs silicone oil) flow from S to L in the AVGGTs, which were tilted at different angles, 2.3, 3.4, and 5.4° (Movie S5); 4 μL droplets (10cs silicone oil) flow from S to L in the AVGGTs, which were tilted at different angles, 9.3 and 12.1° (Movie S6); droplets flow separately from L to S in two different directions in the designed AVGGT with large outside and small middle diameters (Movie S7) (ZIP)

■ AUTHOR INFORMATION

Corresponding Authors

Di Wu − *Microgravity Key Laboratory, Institute of Mechanics, Chinese Academy of Sciences, Beijing 100190, China*; Email: wudi@imech.ac.cn

Kui Song − *School of Mechanical Engineering and Mechanics, Xiangtan University, Xiangtan 411105, China; Institute of Rheological Mechanics, Xiangtan University, Xiangtan 411105, China*; orcid.org/0000-0001-6296-2369; Email: songkui@xtu.edu.cn

Authors

Zhiqiang Xiao − *School of Mechanical Engineering and Mechanics, Xiangtan University, Xiangtan 411105, China*

Xiaoling Hu − *School of Mechanical Engineering and Mechanics, Xiangtan University, Xiangtan 411105, China; Institute of Rheological Mechanics, Xiangtan University, Xiangtan 411105, China*

Complete contact information is available at: https://pubs.acs.org/10.1021/acs.langmuir.3c00746

Notes

The authors declare no competing financial interest.

■ ACKNOWLEDGMENTS

The authors would like to thank Professor Qi Kang and Professor Li Duan, who are from the Microgravity Key Laboratory, Institute of Mechanics, Chinese Academy of Sciences, for their support with some of the experiments in this work. This research work is supported by the National Natural Science Foundation of China (No. 12172320), the Research Foundation of Education Bureau of Hunan Province (Nos. 20B558, 20C1756), and the Natural Science Foundation of Hunan Province (No. 2021JJ30642).

■ REFERENCES

(1) Li, J.; Guo, Z. G. Spontaneous directional transportations of water droplets on surfaces driven by gradient structures. *Nanoscale* **2018**, *10*, 13814−13831.

(2) Li, J. Q.; Song, Y. X.; Zheng, H. X.; Feng, S. L.; Xu, W. H.; Wang, Z. K. Designing biomimetic liquid diodes. *Soft Matter* **2019**, *15*, 1902−1915.

(3) Li, J.; Hou, Y. M.; Liu, Y. H.; Hao, C. L.; Li, M. F.; Chaudhury, M. K.; Yao, S. H.; Wang, Z. K. Directional transport of high-temperature Janus droplets mediated by structural topography. *Nat. Phys.* **2016**, *12*, 606−612.

(4) Ghazimirsaeed, E.; Madadelahi, M.; Dizani, M.; Shamloo, A. Secondary Flows, Mixing, and Chemical Reaction Analysis of Droplet-Based Flow inside Serpentine Microchannels with Different Cross Sections. *Langmuir* **2021**, *37*, 5118−5130.

(5) Ertsgaard, C. T.; Yoo, D.; Christenson, P. R.; Klemme, D. J.; Oh, S. H. Open-channel microfluidics via resonant wireless power transfer. *Nat. Commun.* **2022**, *13*, No. 1869.

(6) Luo, C.; Mrinal, M.; Wang, X. Self-propulsion of Leidenfrost Drops between Non-Parallel Structures. *Sci. Rep.* **2017**, *7*, No. 12018.

(7) Huang, G. H.; Wei, X.; Gu, Y. H.; Kang, Z.; Lao, L. H.; Li, L.; Fan, J. T.; Shou, D. H. Heterogeneously engineered porous media for directional and asymmetric liquid transport. *Cell Rep. Phys. Sci.* **2022**, *3*, No. 100710.

(8) Yang, X. L.; Liu, X.; Lu, Y.; Song, J. L.; Huang, S.; Zhou, S. N.; Jin, Z. J.; Xu, W. J. Controllable Water Adhesion and Anisotropic Sliding on Patterned Superhydrophobic Surface for Droplet Manipulation. *J. Phys. Chem. C* **2016**, *120*, 7233−7240.

(9) Yang, X.; Zhuang, K.; Lu, Y.; Wang, X. Creation of topological ultraslippery surfaces for droplet motion control. *ACS Nano* **2021**, *15*, 2589−2599.

(10) Box, F.; Thorogood, C.; Hui Guan, J. Guided droplet transport on synthetic slippery surfaces inspired by a pitcher plant. *J. R. Soc. Interface* **2019**, *16*, No. 20190323.

(11) Rubega, M. A. Surface tension prey transport in shorebirds: How widespread is it? *Ibis* **1997**, *139*, 488−493.

(12) Prakash, M.; Quere, D.; Bush, J. W. M. Surface tension transport of prey by feeding shorebirds: the capillary ratchet. *Science* **2008**, *320*, 931−934.

(13) Zheng, Y. M.; Bai, H.; Huang, Z. B.; Tian, X. L.; Nie, F. Q.; Zhao, Y.; Zhai, J.; Jiang, L. Directional water collection on wetted spider silk. *Nature* **2010**, *463*, 640−643.

(14) Wu, D.; Wang, J. N.; Wu, S. Z.; Chen, Q. D.; Zhao, S. A.; Zhang, H.; Sun, H. B.; Jiang, L. Three-Level Biomimetic Rice-Leaf Surfaces with Controllable Anisotropic Sliding. *Adv. Funct. Mater.* **2011**, *21*, 2927−2932.

(15) Chen, H. W.; Zhang, P. F.; Zhang, L. W.; Iu, H. L. L.; Jiang, Y.; Zhang, D. Y.; Han, Z. W.; Jiang, L. Continuous directional water transport on the peristome surface of Nepenthes alata. *Nature* **2016**, *532*, 85−89.

(16) Jiao, Y. L.; Li, C. Z.; Wu, S. Z.; Hu, Y. L.; Li, J. W.; Yang, L.; Wu, D.; Chu, J. R. Switchable Underwater Bubble Wettability on Laser-Induced Titanium Multiscale Micro-/Nanostructures by Vertically Crossed Scanning. *ACS Appl. Mater. Interfaces* **2018**, *10*, 16867−16873.

(17) Wu, J. R.; Yin, K.; Li, L. M.; Wu, Z. P.; Xiao, S.; Wang, H.; Duan, J. A.; He, J. Under-oil self-driven and directional transport of water on a femtosecond laser-processed superhydrophilic geometry-gradient structure. *Nanoscale* **2020**, *12*, 4077−4084.

(18) Ji, J. W.; Jiao, Y. L.; Song, Q. R.; Zhang, Y.; Liu, X. J.; Liu, K. Bioinspired Geometry-Gradient Metal Slippery Surface by One-Step Laser Ablation for Continuous Liquid Directional Self-Transport. *Langmuir* **2021**, *37*, 5436−5444.

(19) Jiao, Y. L.; Li, C. Z.; Lv, X. D.; Zhang, Y. Y.; Wu, S. Z.; Chen, C.; Hu, Y. L.; Li, J. W.; Wu, D.; Chu, J. R. In situ tunable bubble wettability with fast response induced by solution surface tension. *J. Mater. Chem. A* **2018**, *6*, 20878−20886.
(20) Wang, L.; Yin, K.; Deng, Q.; Huang, Q.; He, J.; Duan, J.-A. Wetting Ridge-Guided Directional Water Self-Transport. *Adv. Sci.* **2022**, *9*, No. 2204891.
(21) He, Y.; Wang, L.; Wu, T.; Wu, Z.; Chen, Y.; Yin, K. Facile fabrication of hierarchical textures for substrate-independent and durable superhydrophobic surfaces. *Nanoscale* **2022**, *14*, 9392−9400.
(22) Wu, Z.; Yin, K.; Wu, J.; Zhu, Z.; Duan, J.-A.; He, J. Recent advances in femtosecond laser-structured Janus membranes with asymmetric surface wettability. *Nanoscale* **2021**, *13*, 2209−2226.
(23) Yin, K.; Wu, Z.; Wu, J.; Zhu, Z.; Zhang, F.; Duan, J.-A. Solar-driven thermal-wind synergistic effect on laser-textured superhydrophilic copper foam architectures for ultrahigh efficient vapor generation. *Appl. Phys. Lett.* **2021**, *118*, No. 211905.
(24) Kumar, M.; Bhardwaj, R.; Sahu, K. C. Wetting Dynamics of a Water Droplet on Micropillar Surfaces with Radially Varying Pitches. *Langmuir* **2020**, *36*, 5312−5323.
(25) Gorthi, S. R.; Mondal, P. K.; Biswas, G.; Sahu, K. C. Electrocapillary filling in a microchannel under the influence of magnetic and electric fields. *Can. J. Chem. Eng.* **2021**, *99*, 725−741.
(26) Randive, P.; Dalal, A.; Sahu, K. C.; Biswas, G.; Mukherjee, P. P. Wettability effects on contact line dynamics of droplet motion in an inclined channel. *Phys. Rev. E* **2015**, *91*, No. 053006.
(27) Xu, Z.-L.; Chen, J.-Y.; Liu, H.-R.; Sahu, K. C.; Ding, H. Motion of self-rewetting drop on a substrate with a constant temperature gradient. *J. Fluid Mech.* **2021**, *915*, No. A116.
(28) McCuan, J. Symmetry via spherical reflection and spanning drops in a wedge. *pacific journal of mathematics* **1997**, *180*, 291−323.
(29) Concus, P.; Finn, R. Discontinuous behavior of liquids between parallel and tilted plates. *Phys. Fluids* **1998**, *10*, 39−43.
(30) Luo, C.; Heng, X.; Xiang, M. M. Behavior of a Liquid Drop between Two Nonparallel Plates. *Langmuir* **2014**, *30*, 8373−8380.
(31) Zhuang, K.; Lu, Y.; Wang, X. L.; Yang, X. L. Architecture-Driven Fast Droplet Transport without Mass Loss. *Langmuir* **2021**, *37*, 12519−12528.
(32) Reyssat, E. Drops and bubbles in wedges. *J. Fluid Mech.* **2014**, *748*, 641−662.
(33) Konda, H.; Kumar Tripathi, M.; Chandra Sahu, K. Bubble Motion in a Converging−Diverging Channel. *J. Fluids Eng.* **2016**, *138*, No. 064501.
(34) Torres, L. J. *Capillary Migration of Large Confined Drops in Non-Wetting Wedges*; Portland State University, 2019.
(35) Sen, U.; Chatterjee, S.; Ganguly, R.; Dodge, R.; Yu, L. S.; Megaridis, C. M. Scaling Laws in Directional Spreading of Droplets on Wettability-Confined Diverging Tracks. *Langmuir* **2018**, *34*, 1899−1907.
(36) Li, J. Q.; Zhou, X. F.; Li, J.; Che, L. F.; Yao, J.; McHale, G.; Chaudhury, M. K.; Wang, Z. K. Topological liquid diode. *Sci. Adv.* **2017**, *3*, No. eaao3530.
(37) Young, W.-B. Analysis of capillary flows in non-uniform cross-sectional capillaries. *Colloid Surf., A* **2004**, *234*, 123−128.
(38) Erickson, D.; Li, D.; Park, C. B. Numerical simulations of capillary-driven flows in nonuniform cross-sectional capillaries. *J Colloid Int. Sci.* **2002**, *250*, 422−430.
(39) Reyssat, M.; Courbin, L.; Reyssat, E.; Stone, H. A. Imbibition in geometries with axial variations. *J. Fluid Mech.* **2008**, *615*, 335−344.
(40) Gorce, J. B.; Hewitt, I. J.; Vella, D. Capillary Imbibition into Converging Tubes: Beating Washburn's Law and the Optimal Imbibition of Liquids. *Langmuir* **2016**, *32*, 1560−1567.
(41) Singh, M.; Kumar, A.; Khan, A. R. Capillary as a liquid diode. *Phys. Rev. Fluids* **2020**, *5*, No. 102101.
(42) Iwamatsu, M. Thermodynamics and hydrodynamics of spontaneous and forced imbibition in conical capillaries: A theoretical study of conical liquid diode. *Phys. Fluids* **2022**, *34*, No. 047119.
(43) Michielsen, S.; Zhang, J. L.; Du, J. M.; Lee, H. J. Gibbs Free Energy of Liquid Drops on Conical Fibers. *Langmuir* **2011**, *27*, 11867−11872.
(44) Dai, R. Y.; Li, G. Q.; Xiao, L.; Li, Y. X.; Cui, Z. H.; Jia, L.; Zhou, M. L.; Song, Y. G.; Yang, Y.; Cai, Y.; Chen, C. F.; Yin, K. A droplet-driven micro-surfboard with dual gradients for programmable motion. *Chem. Eng. J.* **2022**, *446*, No. 136874.
(45) Canny, J. A computational approach to edge detection. *IEEE Trans. Pattern Anal.* **1986**, *PAMI-8*, 679−698.
(46) Mumley, T. E.; Radke, C.; Williams, M. C. Kinetics of liquid/liquid capillary rise: I. Experimental observations. *J. Colloid Int. Sci.* **1986**, *109*, 398−412.
(47) Bradley, A. T.; Box, F.; Hewitt, I. J.; Vella, D. Wettability-independent droplet transport by Bendotaxis. *Phys. Rev. Lett.* **2019**, *122*, No. 074503.
(48) Wong, T.-S.; Kang, S. H.; Tang, S. K.; Smythe, E. J.; Hatton, B. D.; Grinthal, A.; Aizenberg, J. Bioinspired self-repairing slippery surfaces with pressure-stable omniphobicity. *Nature* **2011**, *477*, 443−447.
(49) De Gennes, P.-G.; Brochard-Wyart, F.; Quéré, D. *Capillarity and Wetting Phenomena: Drops, Bubbles, Pearls, Waves*; Springer, 2004; Vol. *315*.
(50) Hoffman, R. L. A study of the advancing interface. I. Interface shape in liquid—gas systems. *J Colloid Int. Sci.* **1975**, *50*, 228−241.
(51) Van Remoortere, P.; Joos, P. The kinetics of wetting: The motion of a three phase contactline in a capillary. *J. Colloid Int. Sci.* **1991**, *141*, 348−359.
(52) Ludviksson, V.; Lightfoot, E. Deformation of advancing menisci. *AIChE J.* **1968**, *14*, 674−677.
(53) Mumley, T. E.; Radke, C.; Williams, M. C. Kinetics of liquid/liquid capillary rise: II. Development and test of theory. *J Colloid Int. Sci.* **1986**, *109*, 413−425.
(54) Gibbs, J. W.The Scientific Paper of J. Williard Gibbs *Thermodynamics* 1961; Vol. *1*, p 55.
(55) Hyun, W. J.; Kumar, S.; Francis, L. F.; Frisbie, C. D. Open-channel microfluidic diodes based on two-tier junctions. *Appl. Phys. Lett.* **2018**, *113*, No. 193701.
(56) Buckingham, E. On physically similar systems; illustrations of the use of dimensional equations. *Phys. Rev.* **1914**, *4*, No. 345.

https://doi.org/10.1021/acs.langmuir.3c00746
Langmuir 2023, 39, 7901−7911